Process Scaling and Transient Melt Pool Size Control in Laser-Based Additive Manufacturing Processes

Andrew Birnbaum, Pruk Aggarangsi and Jack Beuth
Department of Mechanical Engineering
Carnegie Mellon University
Pittsburgh, PA 15213

Abstract

This modeling research considers two issues related to the control of melt pool size in laser-based additive manufacturing processes. First, the problem of process size scale is considered, with the goal of applying knowledge developed at one processing size scale (e.g. the LENS™ process, using a 500 watt laser) to similar processes operating at larger scales (e.g. a 3 kilowatt system under development at South Dakota School of Mines and Technology). The second problem considered is the transient behavior of melt pool size due to a step change in laser power or velocity. Its primary application is to dynamic feedback control of melt pool size by thermal imaging techniques, where model results specify power or velocity changes needed to rapidly achieve a desired melt pool size. Both of these issues are addressed via a process map approach developed by the authors and co-workers. This approach collapses results from a large number of simulations over the full range of practical process variables into plots process engineers can easily use.

Introduction

Substantial progress has been made over the last decade in developing laser-based manufacturing processes for the purposes of solid freeform fabrication, cladding, component repair and additive manufacturing of features onto existing parts. In particular, over roughly the past eight years, an extensive research effort at Sandia National Laboratories to develop the LENS™ process (Griffith et al., 1996) has yielded an understanding of process parameters needed to build a number of standard shapes out of stainless steel, titanium and other alloys. Significant progress has also been made in developing real-time feedback control via thermal imaging of the melt pool (Griffith el at., 1999 and Hofmeister et al., 2001)

Recently, the use of laser-based processes for component repair and additive manufacturing applications has received significant attention in the aerospace industry. In the case of additive manufacturing, significant cost savings are possible in the manufacture of some components if laser-based deposition is used to add small features to larger parts manufactured by traditional processes. For example, the traditional approach for manufacturing aircraft engine casings is to forge them with a thickness roughly twice that of the final casing thickness. Machining is then used to remove large amounts of material, leaving small-scale features on the casing surface. Significant cost savings are possible by instead forging a near-net-thickness engine casing and adding external features via laser deposition.

With the developments described above, two key issues have emerged as critical for the advancement of laser-based additive manufacturing processes. The first is the need for a fundamental understanding of process scaling. Many industrial applications demand the use of large-scale deposition processes, yet significant process development has occurred on small-

scale processes. For instance, the LENS^{TM} process uses a 500 W Nd:YAG laser. In contrast AeroMet, which manufactures components for the aerospace industry, uses an 18 kW CO_2 laser. There is currently no fundamental understanding of how to apply deposition knowledge acquired from small-scale systems to analogous large-scale systems. The result is that whenever a new laser-based manufacturing system is developed at a different size scale, processing engineers have to nearly start from scratch, performing large numbers of experiments to characterize their process.

The second critical issue for laser-based additive manufacturing processes is the need for a fundamental understanding of transient changes in process characteristics such as melt pool size with changes in process variables such as laser power and velocity. This understanding is needed to aid in the real-time feedback control of melt pool size. In particular, an understanding of thermal response times (the time for a step change in power or velocity to produce a desired change in melt pool size) is needed. For example, results presented for thin-walled structures by Aggarangsi et al. (2003) (also in this symposium proceedings) demonstrate that effective control of melt pool size during the approach of a free edge requires initiation of power reductions before melt pool size increases are observed. This is due to the fact that the time needed for the melt pool size to change due to a power reduction is comparable to the time over which the melt pool size increases as the free edge is approached.

The research described in this paper represents an initial attempt at addressing these two issues. Work described herein builds directly on modeling work by Vasinonta et al. (1999, 2001a, 2001b) developing easy-to-use "process maps" allowing the prediction of steady-state melt pool size in thin walled and bulky features for any practical combination of LENS^{TM} process variables. The simultaneous control of residual stress and melt pool size has been addressed by Vasinonta et al. (2000). A brief overview of the process map approach to understanding laser-based freeform fabrication processes is given by Beuth and Klingbeil (2001) and a complete presentation of the process map approach for controlling steady-state melt pool size and residual stress in thin-walled and bulky parts is given by Vasinonta (2002). Most recently, process maps of cooling rates and thermal gradients at the melt pool boundary have been developed with the goal of predicting microstructure (Bontha and Klingbeil, 2003) (also in this symposium proceedings).

The approaches and results from this earlier work can be used by process engineers to determine, in general, how to modify process variables in order to obtain an ideal melt pool size, control maximum residual stresses and control microstructure. However, results from this earlier work are tailored for application to the LENS^{TM} or other similarly sized processes. Also, only steady-state melt pool size control is addressed. In this paper, results are presented which show how a process map approach can be extended to understand melt pool size control over a range of process size scales and to understand the transient response of melt pool size to step changes in laser power or velocity.

Numerical Models and the Process Map Approach

Numerical Models: Both issues addressed in this paper are considered with reference to the 2D thin-walled geometry shown in Fig. 1. The geometry represents a thin-walled structure deposited onto a comparatively large base plate that acts as a heat sink. The models used in this

paper are analogous to models developed by Vasinonta (2002). Models are of a concentrated heat source moving across the top of the thin wall and do not model the effects of material addition. The absorbed laser power is designated as αQ, where α is the fraction of laser power from the source that is absorbed by the thin wall. In comparing with experiments and in determining ranges of absorbed laser powers a value of $\alpha = 0.35$ is used. Predictions from numerical models assuming a value of $\alpha = 0.35$ have shown good agreement with melt pool lengths in thin-walled structures measured via thermal imaging using the LENS^{TM} process (Vasinonta et al., 1999, 2002a). The successive deposition of layers is not modeled, but the preheating effects of the deposition of prior layers can be approximated via the specification of an elevated uniform temperature in the wall and base plate, designated as T_{base}, which exists before the laser begins its travel across the top of the wall. In all cases considered in this paper, the wall is tall enough that any increases in height will not change the results (results are independent of wall height). The issue of sufficient wall heights to achieve this condition is addressed by Vasinonta et al. (1999, 2001a). Similarly, in this study melt pool size results are taken when the heat source is sufficiently far from the vertical free edges that results are independent of the distance from the edges. In the process scaling simulations, processes using large values of laser power were performed with models having length and height dimensions scaled up to ensure that the conditions described above were satisfied. Numerical models for transient response simulations have larger length dimensions than analogous process scaling simulations because steady state conditions must be reached twice during the analyses.

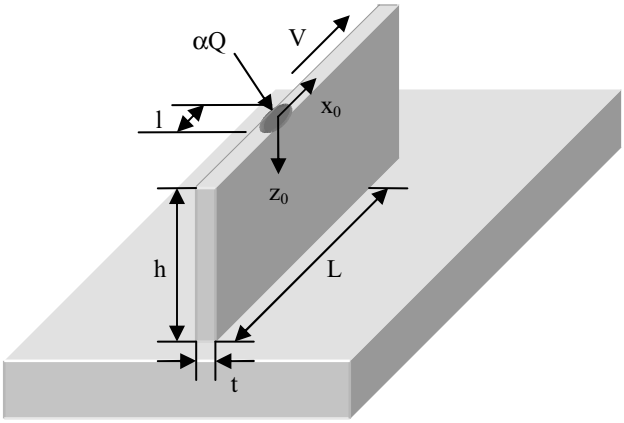

Figure 1 Thin-Walled Structure with Base Plate

Figure 2 shows a typical finite element mesh used for the scaling effects analysis. A similar (but longer) mesh was used for the transient response simulations. The boundary conditions for both types of analyses are thermal insulation on the vertical free edges, as well as the top edge, while a constant temperature is enforced at the bottom edge, simulating the effects of the base plate. Out of plane conduction is also restricted as this is a 2D model. The models use four-node quadrilateral bi-linear elements provided by the ABAQUS finite element package. In going from left to right, there are two separate mesh densities. The first third of the model has fairly coarse resolution while the remaining portion is of significantly finer resolution. This approach was taken to reduce analysis time with the caveat that fine resolution is only required away from the left vertical edge, where melt pool length values are extracted from the model. Mesh resolution also increases as the top edge of the model is approached. For the process scaling simulations, constant power is applied to nodes over pre-determined time steps. Time

steps are specified as equal to the element edge length divided by the heat source velocity. The transient melt pool analysis includes step changes in absorbed laser power and/or velocity.

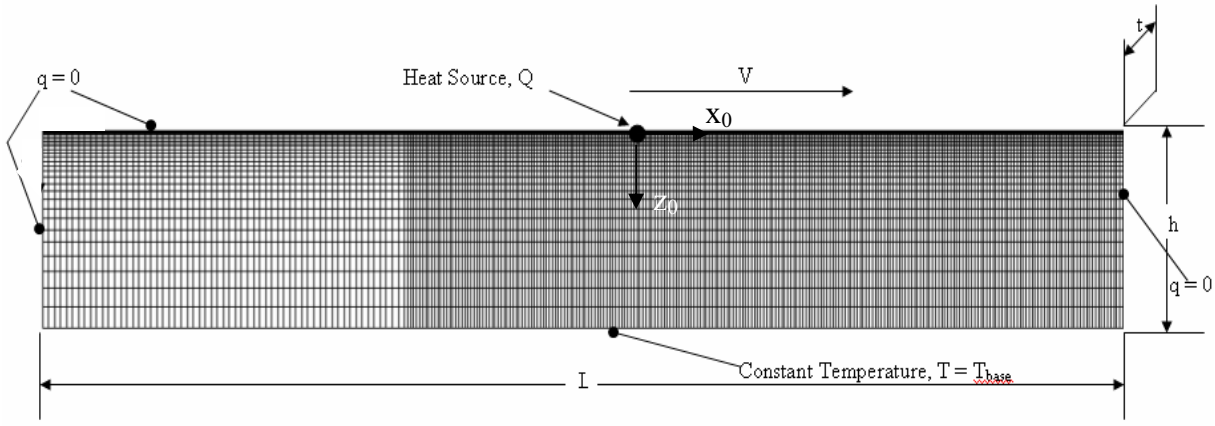

Figure 2 Finite Element Mesh with Boundary Conditions

Thermal properties of AISI 304 stainless steel are used as inputs to the models (Dobranich and Dykhuizen, 1998). A solidus temperature of 1672 K, a liquidus temperature of 1727 K, a latent heat of fusion of 2.65×10^5 J/kg, and a constant density of 7652 kg/m^3 are specified, while temperature dependent thermal conductivity, k and specific heat, c are given by the following linear equations:

$$k = 8.116 + 0.01618(T) \text{ (W/m)} \quad (1)$$
$$c = 465.4 + 0.1336(T) \text{ (J/kgK)}$$

below a temperature of 1500 K. Above 1500 K, both thermal conductivity and specific heat are held constant at the 1500 K value.

Process Map Approach: Because the process scaling and transient analysis research described herein build upon previously developed process map concepts, a brief overview of the earlier research as applied to thin-walled structures is provided here. A process map for melt pool length for a thin-walled structure traversed by a concentrated laser heat source has been developed by Vasinonta et al. (1999, 2001a). As suggested by the Rosenthal (1946) solution for a point heat source moving across a (2-D) half-space, a process map for melt pool length is represented through three dimensionless variables: the normalized melt pool length ($\bar{l}$), the normalized substrate height ($\bar{h}$) and the normalized melting temperature ($\bar{T}_m$) which are defined as follows:

$$\bar{l} = \frac{l}{2k/\rho cV}, \ \bar{h} = \frac{h}{2k/\rho cV} \text{ and } \bar{T}_m = \frac{T_m - T_{base}}{\alpha Q/\pi kt}. \quad (2)$$

In eq. (1), ρ, c and k are the density, specific heat and thermal conductivity, respectively. If thermal properties are temperature-independent, results from the analysis of a concentrated heat source moving over a thin-walled structure of finite height, h, can be represented as a single surface plotted on three coordinate axes of $\bar{l}$, $\bar{h}$ and $\bar{T}_m$. This forms the basis of a process map for laser deposition of thin-walled structures.

The process map for deposition of thin-walled structures of stainless steel 304 via the LENS™ process is shown in Fig. 3. It consists of three surfaces plotted on three coordinate axes. The middle surface was developed from finite element simulations with temperature-independent properties. The results from temperature-dependent property simulations are also presented in Fig. 3 as upper and lower error surfaces that bound the results. The space between these error surfaces reflects the range in results seen when process variables are varied over the range of interest in the LENS™ process.

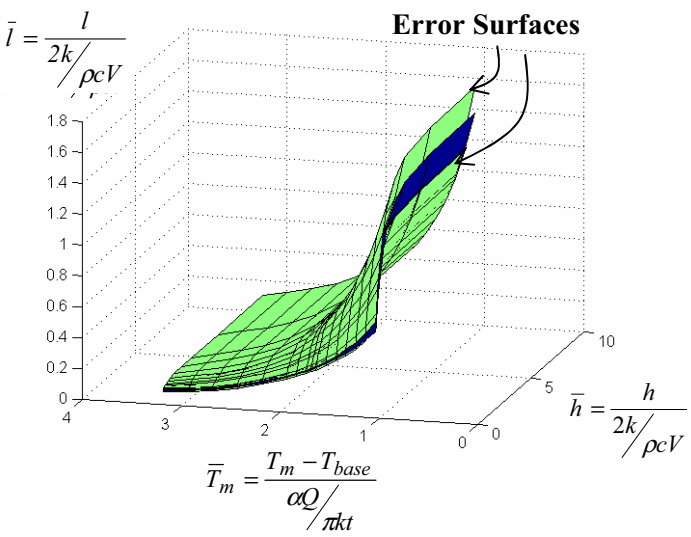

Figure 3 Process Map for Steady-State Melt Pool Length

The plot of Fig. 3 shows that the variability of results due to temperature-dependent properties can be confined to +/-6.5% if certain procedures for applying the process map are followed (Vasinonta et al., 2001a). In brief, these procedures are:

1. Properties at 1000 K are used in the normalizations.
2. For cases involving a change in preheat, a linear change in thermal conductivity with a preheat temperature (in deg. C) is assumed, given by $k = 24.3 + 0.013(T_{base}-30)$ W/(mK).
3. For predicting steady-state melt pool lengths resulting from a change in process variables, wall thickness is assumed to scale proportionally with melt pool length. It is also assumed that the melt pool length/wall thickness scaling is unaffected by velocity.

The third assumption is necessary because the wall thickness, t, is included in the normalized variable $\bar{T}_m$ used in the process map. This requires that some assumption be made regarding the relationship between melt pool length and wall thickness. It also means, however, that within the limits of assumption #3 and given a value of t from a single experiment, the process map can be used to predict not only melt pool lengths as a function of process variables, but also wall thicknesses.

In summary, the process map approach developed in previous work allows the representation of the dependence of melt pool length on absorbed laser power, αQ, laser velocity, V, and wall preheat temperature, T_{base}, in the form of a single, easy-to-use plot in terms of dimensionless variables. The variability of results due to the temperature dependence of material properties can be kept within practical limits. However, the process map of Fig. 3 is specifically developed for the deposition of 304 stainless steel over the range of process variables of interest in

the LENS™ process. Results in the next section of this paper will address methods for extending this approach to other process variable ranges. Also, the process map of Fig. 3 only allows prediction of steady-state melt pool lengths. It gives no information on the rate of change of melt pool length (from one steady-state value to another) if process variables are altered. This is the second major topic addressed in this paper.

Process Scaling

Targeted Manufacturing Process: A laser processing facility is currently under development within the Advanced Materials Processing Center at the South Dakota School of Mines and Technology for use in not only net shape manufacturing but also welding, micro-machining, surface treatment and other applications. The system consists of a 3 kW Nd:YAG laser with a robotic positioning system, dual powder feeders and geometric, temperature and position sensing and feedback control capabilities. It is currently being tested for net shape manufacturing applications through the building of a series of flat, thin-walled structures deposited using laser powers from 450 W to 900 W. These initial tests will be followed up by tests on thin walls and other shapes for powers up to 2700 W. Laser velocities of interest range from 10 to 20 mm/s (Sears et al., 2003).

Because the power range of the laser at the AMP Center is significantly larger than that for the 500 W LENS™ system, the development of this new facility offers a unique opportunity for testing the applicability of a process map approach on multiple process size scales. In the next section, methods are presented for using process map concepts to model melt pool size and wall thickness for processes at multiple scales. Wall thickness predictions from process maps are then compared to available data from the AMP Center in the 450 to 900 W power range. In addition, wall thicknesses are predicted beyond the range of available data, up to a power level of 2700 W, providing researchers at the AMP Center with predictions of wall thicknesses in advance of their experiments.

Process Maps for Multiple Process Scales: In this section, methods are described for extending the process map approach for predicting melt pool length and wall thickness to processes operating at multiple size scales. The earlier work by Vasinonta showed that melt pool length predictions from models of the LENS™ process could be collapsed into a single plot of nondimensional variables if thermal properties at 1000 K are used in the normalization. In this section, it will be shown that processes at larger size scales can be similarly represented if properties at lower temperatures are used in the normalization.

In order to analyze the effects of process scaling, laser powers of 125 W to 2700 W (αQ from 43.8 W to 945 W assuming a value of $\alpha = 0.35$) were divided into three power ranges. The upper range is from 1300 W to 2700 W (αQ from 455 W to 945 W). The middle range has powers from 429 W to 1286 W (αQ from 150 W to 450 W). The lower range is based on the LENS™ process and has powers ranging from 123 W to 471 W (αQ from 43.2 W to 165 W). These ranges were chosen with the goal of maximizing range size, while keeping maximum errors from use of the process map within practical limits.

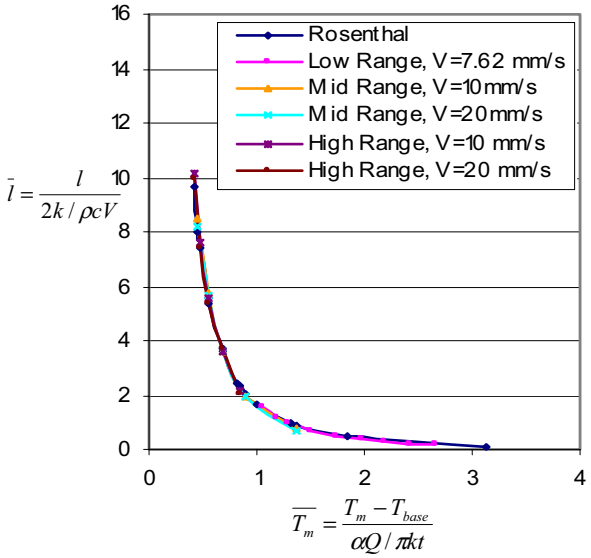

Figure 4 Comparison of Normalized Results with the Rosenthal Solution over Three Power Ranges, Using a Pre-Heat Temperature T_{base} = 303 K

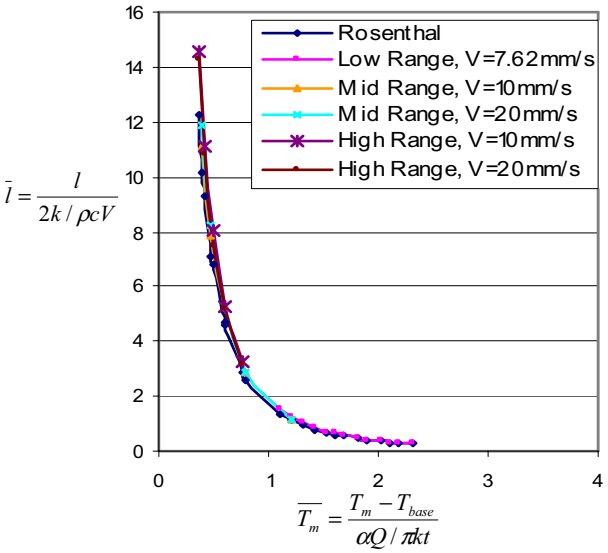

Figure 5 Comparison of Normalized Results with the Rosenthal Solution Over Three Power Ranges, Using a Pre-Heat Temperature T_{base} = 673 K

As in earlier process map work, a single experimental value of the wall thickness, t, is needed to predict values of l and t as a function of absorbed laser power, αQ, laser velocity, V, and wall and base plate preheat temperature, T_{base}. A prediction of melt pool length, l, for the experimental case yields a value of l/t that is used in all subsequent predictions. In the earlier work, because the velocity range of interest was confined to the relatively narrow range of 5.93 to 9.31 mm/s it was assumed that the ratio of l/t was independent of laser velocity. In this section it will be shown that this assumption can give less than satisfactory results over a larger velocity range. Also, as in earlier work, prediction of melt pool length and wall thickness using the process map must be done using an iterative scheme. For instance, a larger value of αQ results in a new (smaller) value of $\overline{T}_m$. That smaller value of $\overline{T}_m$ results in new (larger) values of l and t, but the larger value of t in turn results in a slightly larger value of $\overline{T}_m$. This again leads to new values of l and t. These calculation steps are repeated until $\overline{T}_m$, l and t no longer change significantly.

Figures 4 and 5 provide plots of $\bar{l}$ vs. $\overline{T}_m$ over the three ranges of $\overline{T}_m$ identified above, covering the full range of laser powers from 125 W to 2700 W (αQ from 43.8 W to 945 W) applicable to the LENS™ and AMP Center processes. Because they are for tall walls, the 2-D plots of Figs. 4 and 5 correspond to values from the process map of Fig. 3 for the limiting case of large values of $\bar{h}$. More specifically, data plotted in the low range of powers (large values of $\overline{T}_m$) reproduces the data of Fig. 3 for large $\bar{h}$. Data for smaller values of $\overline{T}_m$ is new and relates to power ranges and velocities appropriate for the AMP Center process. Figure 4 gives results for a value of T_{base} = 303 K and Fig. 5 gives results for an upper bound value of T_{base} = 673 K. In both cases, results are given for the upper and lower bounds of V = 10 mm/s and V = 20 mm/s for the middle and upper power ranges (applicable to the AMP Center process). Results at V = 15 mm/s were also obtained but are not shown because they fall between results for the upper and lower values of velocity.

The plots of Figs. 4 and 5 show that errors can be confined to +/-8% in the upper and middle power ranges if the following procedures for applying the process map are followed:

1. Properties at a normalization temperature $T_{norm} < 1000$ K are used in the normalizations.
2. For cases involving a change in preheat, a linear change in thermal conductivity with a preheat temperature (in deg. C) is assumed, given by $k = k_{Tnorm} + 0.013(T_{base}-30)$ W/(mK), where k_{Tnorm} is the conductivity at the chosen normalization temperature.
3. For predicting steady-state melt pool lengths resulting from a change in process variables, wall thickness is assumed to scale proportionally with melt pool length.

In other words, the process map approach can be applied over multiple process size scales by simply changing the normalization temperature with changes in power range.

Temperatures at which process parameters are normalized by are chosen to minimize errors in the process map (Figs 4 and 5) due to temperature-dependent properties. Figure 6 shows the functional dependence of normalization temperature on median $\overline{T}_m$ values for each power range. The plot can roughly be approximated as linear over the range of $\overline{T}_m$ values considered. It is not clear whether a linear extrapolation to higher powers (lower values of $\overline{T}_m$) would be accurate. However, a linear extrapolation of the curve toward $\overline{T}_m = 0$ (αQ approaching infinity) suggests a normalization temperature near 820 K. This change in normalization temperature would yield relatively small changes in k and c (see equation (1)). This suggests that the modeling of even larger scale processes via a process map approach may be straightforward. It also suggests that the effects of changes in process scale are reduced at higher power ranges and that experimental results from the AMP Center process may provide significant insight into processes operating at significantly larger laser powers.

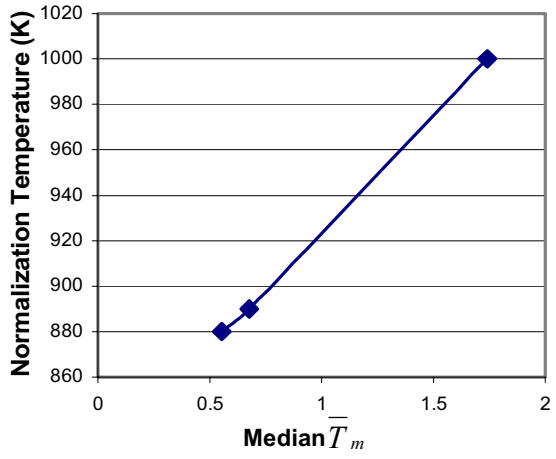

Figure 6 Normalization Temperature as a Function of Median $\overline{T}_m$

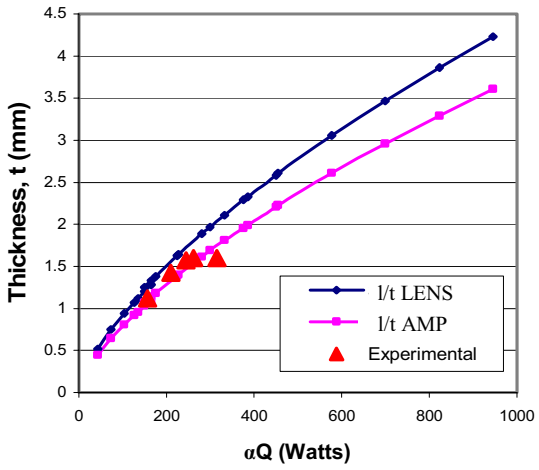

Figure 7 Comparison of Experimental and Predicted Thicknesses as a Function of αQ

Application of the Results: Figure 7 shows a plot of predicted and measured wall thicknesses vs. αQ. Measured values are from the AMP Center process (Sears et al. (2003)) for a laser velocity of 20 mm/s and are shown as large data points. Predictions as a function of αQ and for V = 20

mm/s are shown as plotted lines with small data points. Two sets of predictions are presented. The top line represents process map predictions using an experimental value of t from the LENS™ process for αQ = 105 W and V = 7.62 mm/s to determine l/t. Although the trends in the experiments are captured by these predictions, the predicted values are larger than the experimental values.

This difference can be explained by the use of a value of l/t determined from experiments at a significantly lower velocity than was used in the experiments. This ratio will, in fact, increase with an increase in velocity. The second set of predictions (the lower line) was generated from the same process map results (Figs. 4 and 5), but with a value of t from the AMP process for αQ = 210 W and V = 14 mm/s used to determine l/t. These predictions agree quite well with the available experimental data. Furthermore, the predictions for larger powers could be a useful tool in reducing the number of experiments AMP engineers need to perform while developing their process.

Transient Response of Melt Pool Size

In this section, numerical results are presented for transient changes in melt pool size due to a step change in laser power and/or velocity, for application to feedback control of melt pool size. Furthermore, results are presented in a non-dimensional process map format using the rules outlined in the Process Map Approach section, allowing the results from a large number of simulations to be presented in a compact form. In this section, simulations are for the LENS^{TM} process; however, the same approach could be applied to other laser-based deposition processes.

Figure 8 provides a plot of normalized melt pool length as a function of normalized laser travel distance for multiple values of step changes in laser velocity and/or power. The "baseline" set of initial process variables are αQ = 105 W, V = 7.62 mm/s and T_{base} = 303 K. These variables result in a value of $\overline{T}_m$ = 1.29 and a value of $\bar{l}$ = 1.01. Increases in absorbed laser power per thickness of 10% and 50% and decreases of 10% and 50% have been identified as baseline changes in process variables of interest, resulting in values of $\overline{T}_m$ equal to 1.18, 0.86, 1.44 and 2.59, respectively.

Considering just the baseline set of initial variables and power changes, Fig. 8 shows how normalized melt pool length changes from the steady-state value of 1.01 to other steady-state values as a function of the normalized distance traveled by the laser. Actual values of melt pool length and laser travel distance can be calculated from the normalized values using the properties of SS304 at 1000 K. Furthermore, the distance needed to reach the new steady-state value of melt pool length can be converted to a time to reach steady state by dividing by the laser velocity.

Figure 8 is more than a plot of changes in melt pool length due to step changes in power, however. It is really a plot of normalized melt pool length vs. normalized laser travel distance for the changes in $\overline{T}_m$ shown for any practical combination of process variables. For each $\overline{T}_m$ value, two combinations of process variables αQ, V and T_{base} that give the highest and lowest values of $\bar{l}$ in the steady-state process map were selected, representing upper and lower bound

cases. For all values of $\overline{T}_m$ the upper bound case corresponds to values of T_{base} = 400 °C and the lower bound case corresponds to values of T_{base} = 30 °C. A series of transient simulations were then performed between upper bound cases and between lower bound cases (with T_{base} fixed) for each of the four step changes in $\overline{T}_m$. The results of all of these simulations are plotted in Fig. 8.

Overall, the process map approach developed for steady-state conditions has allowed a compact presentation of transient results over the full range of process variables of interest in LENS™. However, although the steady-state normalized results have an error of no more than +/- 6.5% (designated by the error bars in the figure), transient results are not necessarily confined to these limits. As shown in Fig. 8, distances (or times) needed to transition to a new steady-state melt pool size are greater for decreases in $\overline{T}_m$ (e.g. an increase in power) than for equivalent increases in $\overline{T}_m$. Using the properties of 304 stainless steel at 1000 K and a velocity V = 7.62 mm/s, the conversion between $\bar{x}$ and x is x (in mm) = 1.39 $\bar{x}$. For V = 7.62 mm/s, this gives thermal response times roughly in the range of 0.2 to 1.1 seconds, which is consistent with response times measured via thermal imaging of the LENS™ process.

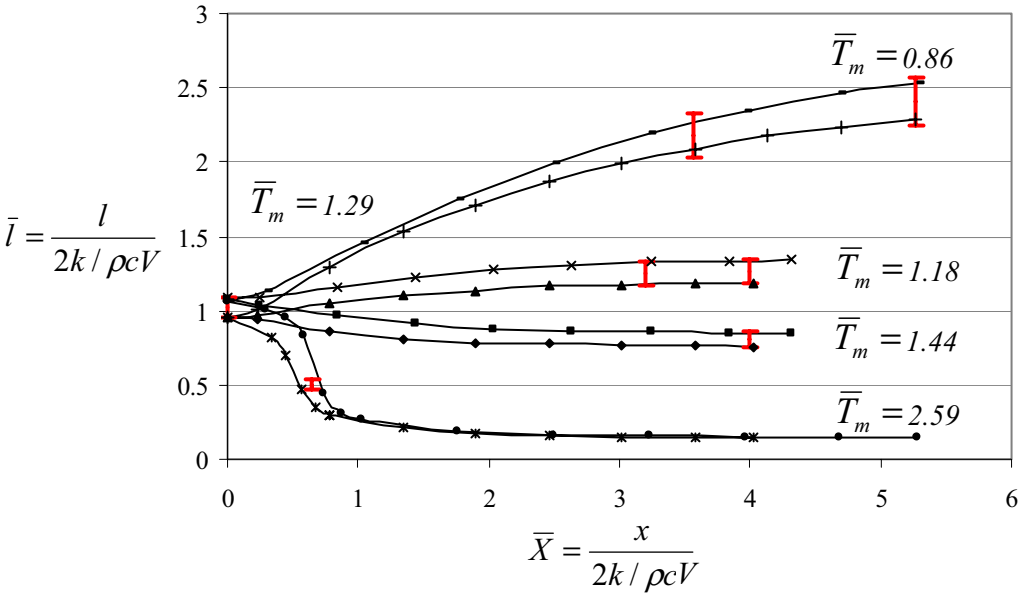

Figure 8 Melt Pool Size Transient Response Process Map with Error Bars Showing a Variation of ±6.5% from the Mean Values

Summary and Conclusions

In this study, process map approaches previously developed for application to the LENS™ process under steady state conditions have been extended to predict transient changes in melt pool length and wall thickness and to predict steady-state melt pool lengths and wall thicknesses for processes on multiple size scales. Results thus far have been limited to thin-walled structures; however, these concepts should be extendable to other common geometries. Process scaling predictions of wall thicknesses have been made for the full power range of a large-scale process currently under development and predictions have compared well to thicknesses measured to date. Predictions of transient changes in melt pool size for the LENS™

process are also consistent with observations of transient melt pool size via thermal imaging. Results have confirmed the applicability of a process map approach to understanding transient behavior; however, error limits under transient conditions may not match those observed in steady-state models. Melt pool size thermal response times for LENS™ range approximately from 0.2 to 1.1 seconds. This sets a lower bound on response times for melt pool size thermal feedback control systems.

Acknowledgements

This research was supported by the National Science Foundation Division of Design, Manufacture and Industrial Innovation, through the Materials Processing and Manufacturing Program, award number DMI-0200270. The authors would like to thank Dave Alexander and Ralph Anderson of Pratt & Whitney for their insights and effort in guiding the industrial applications of this research. The authors are also grateful for to Jim Sears of the South Dakota School of Mines and Technology and Michelle Griffith of Sandia National Laboratories for the important experimental data they have provided.

References

1. Aggarangsi, P., Beuth, J.L., and Griffith, M.L., 2003, “Melt Pool Size and Stress Control for Laser-Based Deposition Near a Free Edge, ” *Solid Freeform Fabrication Proceedings* (D.L. Bourell, J.J. Beaman, H.L. Marcus, R.H. Crawford and J.W. Barlow, eds.), Proc. 2003 Solid Freeform Fabrication Symposium, Austin, August 2003 (this symposium).
2. Beuth, J.L. and Klingbeil, N.W., 2001, "The Role of Process Variables in Laser-Based Direct Metal Solid Freeform Fabrication," *JOM,* September 2001, pp. 36-39.
3. Bontha, S. and Klingbeil, N.W., 2003, “Thermal Process Maps for Controlling Microstructure in Laser-Based Solid Freeform Fabrication,” *Solid Freeform Fabrication Proceedings* (D.L. Bourell, J.J. Beaman, H.L. Marcus, R.H. Crawford and J.W. Barlow, eds.), Proc. 2003 Solid Freeform Fabrication Symposium, Austin, August 2003 (this symposium).
4. Dobranich, D. and Dykhuizen, R.C., 1998, “Scoping Thermal Calculation of the LENS Process,” Sandia National Laboratories Internal Report.
5. Griffith, M.L., Keicher, D.M., Atwood, C.L., Romero, J.A., Smugeresky, J.E., Harwell, L.D. and Greene, D.L., 1996, “Freeform Fabrication of Metallic Components Using Laser Engineered Net Shaping (LENS),” *Solid Freeform Fabrication Proceedings* (D.L. Bourell, J.J. Beaman, H.L. Marcus, R.H. Crawford and J.W. Barlow, eds.), Proc. 1996 Solid Freeform Fabrication Symposium, Austin, August 1996, pp. 125-132.
6. Griffith, M. L., Schlienger, M. E., Harwell, L. D., Oliver, M. S., Baldwin, M. D., Ensz, M. T., Smugeresky, J. E., Essien, M., Brooks, J., Robino, C. V., Hofmeister, W. H., Wert, M. J. and Nelson, D. V., 1999, “Understanding Thermal Behavior in the LENS™ Process,” *Journal of Materials Design,* Vol. 20, No. 2/3 pp. 107-114.
7. Hofmeister, W.H., Griffith, M.L., Ensz, M.T. and Smugeresky, J.E., 2001, "Solidification in Direct Metal Deposition by LENS Processing," *JOM*, Vol. 53, No. 9, 2001, pp. 30-34.
8. Rosenthal, D., 1946,“The Theory of Moving Sources of Heat and Its Application to Metal Treatments,” *Transactions of ASME,* Vol. 68, 1946, pp. 849-866.
9. Sears, J.W., Marquis, F., Arbegast, W. and Langerman, M., 2003, personal communication.
10. Vasinonta, A., Beuth, J. L. and Griffith, M. L., 1999, “Process Maps for Laser Deposition of Thin-Walled Structures,” *Solid Freeform Fabrication Proceedings (*D.L. Bourell, J.J.

Beaman, R. H. Crawford, H. L. Marcus and J. W. Barlow, eds.), Proc. 1999 Solid Freeform Fabrication Symposium, Austin, August 1999, pp. 383-391.
11. Vasinonta, A., Beuth, J.L. and Griffith, M.L., 2000, "Process Maps for Controlling Residual Stress and Melt Pool Size in Laser-Based SFF Processes," *Solid Freeform Fabrication Proceedings* (D.L. Bourell, J.J. Beaman, R.H. Crawford, H.L. Marcus and J.W. Barlow, eds.), Proc. 2000 Solid Freeform Fabrication Symposium, Austin, August 2000, pp. 200-208.
12. Vasinonta, A., Beuth, J. L. and Griffith, M. L., 2001a, "A Process Map for Consistent Build Conditions in the Solid Freeform Fabrication of Thin-Walled Structures," *Journal of Manufacturing Science and Engineering.* Vol. 123, pp. 615-622.
13. Vasinonta, A., Beuth, J.L., and Ong, R., 2001b, "Melt Pool Size Control in Thin-Walled and Bulky Parts via Process Maps," *Solid Freeform Fabrication Proceedings* (D.L. Bourell, J.J. Beaman, R.H. Crawford, H.L. Marcus, K.L. Wood and J.W. Barlow, eds.), Proc. 2001 Solid Freeform Fabrication Symposium, Austin, August 2001, pp. 432-440.
14. Vasinonta, A., 2002, "Process Maps for Melt Pool Size and Residual Stress in Laser-Based Solid Freeform Fabrication," Ph.D. Thesis, Carnegie Mellon University, May 2002.